Electromagnetic Radiation from Organic Light-emitting Diodes

A. Epstein, N. Tessler, and P. D. Einziger
Department of Electrical Engineering, Technion — Israel Institute of Technology
Haifa 32000, Israel

Abstract— An analytical prototype model for the electromagnetic radiation emitted from a nanometric organic light-emitting diode device is presented and thoroughly investigated herein. The results are obtained via asymptotic evaluation of the resultant radiation integral in conjunction with coherence considerations, resulting in closed-form analytical expressions. For the sake of simplicity and clarity, we focus on a two-dimensional canonical configuration excited by impulsive (line) sources. The resultant expressions can be most effectively utilized by engineers for improved design, as they enable the calculation of the device's physical parameters, such as electrical to optical conversion efficiency and emission angular distribution, as a function of device structure. It should be pointed out that the incorporation of both rigorous electromagnetic analysis and coherence effects is addressed in our report, to the best of our knowledge, for the first time. This results in a precise model capable of repeating and interpreting experimental and simulated data.

1. INTRODUCTION

Organic light emitting diodes (OLEDs) have been intensively investigated for the past two decades as potentially promising candidates for the fabrication of thin and flexible displays as well as other novel optoelectronic devices [1–4]. The relatively simple and cheap manufacturing procedures involved in OLED production, the prospects for wide viewing angle and high luminescence as in inorganic LEDs and the fast response compared to liquid crystal displays (LCDs) have made OLED technology a very attractive one [1, 4]. In recent years a major technological effort has been made in order to design durable efficient OLEDs with wide viewing angle [3, 5–7].

Electromagnetic modeling of OLEDs is crucially important for analysis and synthesis of their radiation pattern and radiation efficiency, thereby determining the devices' performance. Indeed, vast research in the past few years aimed at optical modeling of OLEDs in order to achieve an understanding of how the layer dimensions and material composition alter their electromagnetic properties [5–10].

Most of these attempts rely on the early work of Chance, Prock and Silbey [11] (CPS) which showed that a radiatively decaying excited molecule can be modeled by a classical oscillating dipole, and presented integral expressions for the radiative and non-radiative decay rates of such dipole when embedded in layered media, from which the radiation efficiency is readily achieved. The CPS model uses the Hertz vectors formalism and later the dyadic Green function method [12] to express the possible source excitations and apply the layered media constraints on the electromagnetic fields. Numerically evaluating the integral expressions, they found good agreement between simulation and experimental results for fluorescence lifetime of molecules near metallic interfaces.

The intimate connection between the radiation pattern and coherence properties of the radiation source is widely studied by Wolf, and well summarized in [13]. Intuitively speaking, it is clear that sharp interference patterns in emission angular distribution as well as interference fringes on a distant screen are caused by some consistent phase difference between two sources. As temporal or spatial coherence decrease this phase difference is no longer consistent in time or space, thus averaging on a large ensemble of sources diminishes these effects dramatically.

In this paper we present a rigorous electromagnetic analysis of two-dimensional OLED radiation. The basis of our analysis is the decomposition of the source term into its plane-wave spectrum [12, 14, 15], a method which preserves the fundamental physical intuition of plane-wave optics. Asymptotic evaluation of the resultant radiation integral leads to closed-form analytical expressions, which, along with the plane-wave interpretation, enables clear identification of dominant factors which determine the device's radiation pattern properties. The coherence effects are explicitly incorporated in the electromagnetic model and their impact is readily observed in the simulated results, outlined in Sections 2 and 3, respectively.

2. FORMULATION

Let us consider a two-dimensional device with $M + N + 2$ layers, with a line source embedded at a certain plane, $z = z'$, sandwiched between layers (-1) and $(+1)$, as depicted in Fig. 1. The homogeneous layer formed by combining layers (-1) and $(+1)$, containing the line source, is termed the active layer. Each layer is characterized by its permittivity, permeability, and conductivity marked ε_n, μ_n and σ_n, respectively, for the n-th layer. Furthermore, the n-th and $(n+1)$-th layers are separated by the plane $z = d_n$ for $n > 0$ and $z = d_{n+1}$ for $n < 0$. Note that $\varepsilon_{-1} = \varepsilon_1$, $\mu_{-1} = \mu_1$, and $\sigma_{-1} = \sigma_1$. For the sake of completeness, we treat here both transverse electric (TE) and transverse magnetic (TM) modes, excited via electric line source and magnetic line source (Fig. 1), respectively. Throughout the entire paper we use e and m left superscripts or subscripts to denote electric or magnetic cases, respectively. Both sources are assumed to be time harmonic, with time dependence of $e^{j\omega t}$. The wave number and wave impedance of the n-th layer are given as

$$k_n = \omega\sqrt{\mu_n\varepsilon_n\left[1 - j\sigma_n/\left(\omega\varepsilon_n\right)\right]} = \left(\omega/c\right)\left(\mathrm{n}_n - j\kappa_n\right), \qquad Z_n = \sqrt{\mu_n/\left\{\varepsilon_n\left[1 - j\sigma_n/\left(\omega\varepsilon_n\right)\right]\right\}}, \quad (1)$$

where c, n and κ denote the velocity of light in vacuum, refractive index and extinction coefficient, respectively. To satisfy the radiation condition we require $\Im\{k_n\} \le 0$, leading to $\Im\{Z_n\} \ge 0$. Furthermore we define the two-dimensional space vector, $\vec{\rho} = \rho_t\hat{t} + z\hat{z} = \left(-\rho\sin\theta\right)\hat{t} + \left(\rho\cos\theta\right)\hat{z}$, where ρ_t and $\hat{t}$ are its transverse coordinate magnitude and direction, and θ is the angle between the z-axis and $\vec{\rho}$. The transverse coordinate is different for the electric and magnetic cases due to the different symmetry they induce. In the electric line source scenario, there is no change along the x direction, therefore ${}^e[\partial/\partial x] = 0$, ${}^e\rho_t = y$ and ${}^e\hat{t} = \hat{y}$. Analogously, for the magnetic line source scenario we have symmetry along the y-axis, thus, ${}^m[\partial/\partial y] = 0$, ${}^m\rho_t = x$ and ${}^m\hat{t} = \hat{x}$. The source vector in both cases is $\vec{\rho}' = z'\hat{z}$.

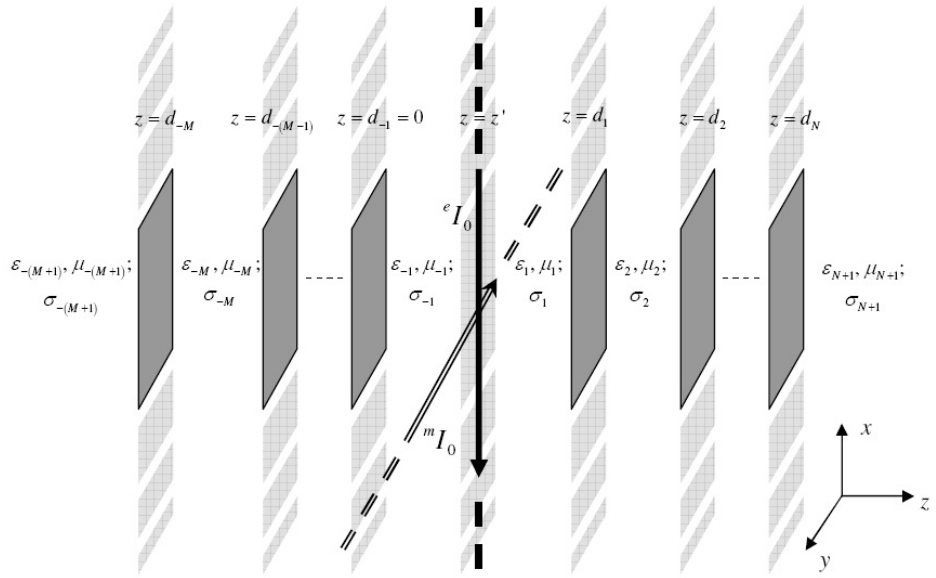

Figure 1: Two-dimensional configuration for the OLED model. The device consists of $M + N + 2$ layers, the interfaces of which are planes parallel to the $\widehat{xy}$ plane and the propagation direction is $\hat{z}$. The two-dimensional model excitation is a line source, sandwiched between layers (-1) and $(+1)$, which form together the active layer.

The transverse electromagnetic field components can be expressed [15] via the following spectral integrals

$$E_x\left(\vec{\rho}, \vec{\rho}'\right) = \frac{1}{2\pi}\int_{-\infty}^{\infty} e_x\left(z, z'\right)\cdot e^{j\vec{k}_t\cdot\vec{\rho}}, \qquad H_y(\vec{\rho}, \vec{\rho}') = \frac{1}{2\pi}\int_{-\infty}^{\infty} h_y\left(z, z'\right)\cdot e^{j\vec{k}_t\cdot\vec{\rho}}, \quad (2)$$

where $e_x(z, z')$, $h_y(z, z')$ and $\vec{k}_t = k_t\hat{t}$, denote the plane-wave spectrum and transverse wave vector, respectively. The transverse plan-wave spectral amplitudes can be readily expressed in terms of

the one-dimensional Green's function, $g(z,z')$,

$$e_x(z,z') = j\beta\widetilde{Z}J_s g(z,z') - M_s\frac{dg(z,z')}{dz}, \qquad h_y(z,z') = -J_s\frac{dg(z,z')}{dz} + j\beta\widetilde{Y}M_s g(z,z'), \tag{3}$$

where

$${}^{e}_{m}\widetilde{Z} = 1/{}^{e}_{m}\widetilde{Y} = Z(k/\beta)^{\pm 1} \quad \text{and} \qquad {}^{e}J_s = {}^{e}I_0, \quad {}^{m}M_s = {}^{m}I_0, \quad {}^{m}J_s = {}^{e}M_s = 0. \tag{4}$$

The wave equation and associated constraints for $g(z,z')$ are outlined in [12, 14, 15]. Note that $g_n(z,z')$ specifies $g(z,z')$ at the n-th layer. Expanding the work presented in [14] we express the Green function in the various layers in terms of reflection, transmission and source coefficients, as demonstrated in Table 1. The recursive expressions for the total reflection and transmission coefficients are derived via the constraints listed in [15], to the right (forward) and to the left (reversed) of the active layer, for both electric and magnetic polarizations.

Table 1: Recursive relations of the one-dimensional Green function.

	Forward Direction ($z > z'$)	Reversed Direction ($z < z'$)
One-dimensional Green function	$g_n(z,z') = \frac{e^{j\beta_1 z'}}{2j\beta_n}\cdot \frac{1-\hat{R}_{-1}(k_t)\,e^{-2j\beta_1 z'}}{1-R_1(k_t)\,\hat{R}_{-1}(k_t)}\left[\prod_{p=2}^{n}T_p(k_t)\right]\left[e^{-j\beta_n z} - R_n(k_t)\,e^{j\beta_n z}\right]$	$g_n(z,z') = \frac{e^{-j\beta_1 z'}}{2j\beta_n}\cdot \frac{1-R_1(k_t)\,e^{2j\beta_1 z'}}{1-R_1(k_t)\,\hat{R}_{-1}(k_t)}\left[\prod_{p=n}^{-2}\hat{T}_p(k_t)\right]\left[e^{j\beta_n z} - \hat{R}_n(k_t)\,e^{-j\beta_n z}\right]$
Total reflection coefficient	$R_n(k_t) = \left\{\Gamma_n(k_t) + \frac{\left[1-\Gamma_n^2(k_t)\right]R_{n+1}(k_t)\,e^{2j\beta_{n+1}d_n}}{1+\Gamma_n(k_t)R_{n+1}(k_t)\,e^{2j\beta_{n+1}d_n}}\right\}e^{-2j\beta_n d_n}$	$\hat{R}_n(k_t) = \left\{\hat{\Gamma}_n(k_t) + \frac{\left[1-\hat{\Gamma}_n^2(k_t)\right]\hat{R}_{n-1}(k_t)\,e^{-2j\beta_{n-1}d_n}}{1+\Gamma_n(k_t)\hat{R}_{n-1}(k_t)\,e^{-2j\beta_{n-1}d_n}}\right\}e^{2j\beta_n d_n}$
Recursion base condition	$R_{N+1}(k_t) = 0$	$\hat{R}_{-(M+1)}(k_t) = 0$
Total transmission coefficient	$T_n(k_t) = \frac{\left[1+\Gamma_{n-1}(k_t)\right]e^{j\left(\beta_n-\beta_{n-1}\right)d_{n-1}}}{1+\Gamma_{n-1}(k_t)R_n(k_t)\,e^{2j\beta_n d_{n-1}}}$	$\hat{T}_n(k_t) = \frac{\left[1+\hat{\Gamma}_{n+1}(k_t)\right]e^{-j\left(\beta_n-\beta_{n+1}\right)d_{n+1}}}{1+\hat{\Gamma}_{n+1}(k_t)\hat{R}_n(k_t)\,e^{-2j\beta_n d_{n+1}}}$
Local reflection coefficient	$\Gamma_n = \frac{1-\gamma_n}{1+\gamma_n}$	$\hat{\Gamma}_n = -\Gamma_{n-1} = \frac{1-\hat{\gamma}_n}{1+\hat{\gamma}_n}$
Impedance ratio	${}^{e}_{m}\gamma_n = \left(\frac{\bar{Z}_{n+1}}{\bar{Z}_n}\right)^{\pm 1}$	${}^{e}_{m}\hat{\gamma}_n = 1/{}^{e}_{m}\gamma_{n-1} = \left(\frac{\bar{Z}_{n-1}}{\bar{Z}_n}\right)^{\pm 1}$

Power relations associated with our OLED layered model are crucially important for evaluating and optimizing the device performance. The most significant relations are the so-called radiation (emission) pattern, radiation power and absorption power, given via

$$S_\rho(\theta,\omega) = \frac{1}{2}\left[\vec{E}\left(\vec{\rho},\vec{\rho}\,'\right)\times\vec{H}^*\left(\vec{\rho},\vec{\rho}\,'\right)\right]\cdot\hat{\rho}\Big|_{\rho\to\infty}, \tag{5}$$

$$S_r(z,\omega) = \int_{-\infty}^{\infty}dy\left\{\frac{1}{2}\left[\vec{E}\left(\vec{\rho},\vec{\rho}\,'\right)\times\vec{H}^*\left(\vec{\rho},\vec{\rho}\,'\right)\right]\cdot\hat{z}\Big|_{z>z'}\right\} \tag{6}$$

and

$$S_a(z,\omega) = \int_{-\infty}^{\infty}dy\left\{\frac{1}{2}\left[\vec{E}\left(\vec{\rho},\vec{\rho}\,'\right)\times\vec{H}^*\left(\vec{\rho},\vec{\rho}\,'\right)\right]\cdot(-\hat{z})\Big|_{z<z'}\right\}, \tag{7}$$

respectively. Substituting (2)–(3) in conjunction with Table 1 into (5)–(7) renders closed-form expressions for the power relations, as summarized in Table 2.

Apparently, coherence effects must be considered when analyzing OLED device, as may be concluded from [9, 10]. Since spatial coherence can, in general, be neglected when considering

OLEDs [16], we take into consideration only the temporal coherence effect on the power relation [13], i.e.,

$$\mathcal{S}(\vec{\rho}) = \int_0^\infty p(\omega)\, S(\vec{\rho},\omega)\, d\omega \tag{8}$$

where $S(\vec{\rho},\omega)$ denotes any of the power relations given in (5)–(7), and $p(\omega)$ is the coherence function of the device, i.e., the appropriately normalized free-space photoluminescence (PL) spectrum. The Gaussian distribution, being simple analytic and effectively bounded function, is selected as the coherence function for our simulations. The Gaussian width, $\Delta\omega$, is inversely proportional to the coherence length [13], L_c, given via, $L_c = 2\pi c/\Delta\omega = \lambda^2/\Delta\lambda$.

Table 2: Power relations for the OLED model. The line source power, P_n, denotes the radiation power of a line source in an unbounded homogeneous medium (the n-th layer).

Radiation pattern, Eq. (5)	$S_\rho(\theta,\omega) = \frac{P_{N+1}}{\pi\rho}\left\lvert\left\{\frac{e^{j\beta_1 z'} - \widehat{R}_{-1}(k_t)\, e^{-j\beta_1 z'}}{1 - R_1(k_t)\,\widehat{R}_{-1}(k_t)}\left[\prod_{p=2}^{N+1} T_p(k_t)\right]\right\}\right\rvert_{k_t = k_{N+1}\sin\theta}\right\rvert^2$
Radiation power, Eq. (6)	$S_r^n(z,\omega) = \frac{P_n}{\pi}\int_{-\infty}^{\infty} dk_t \left\{\frac{e^{2\Im\{\beta_n\}z}}{\beta_n}\left\lvert\frac{e^{j\beta_1 z'} - \widehat{R}_{-1}(k_t)\, e^{-j\beta_1 z'}}{1 - R_1(k_t)\,\widehat{R}_{-1}(k_t)}\left[\prod_{p=2}^{n} T_p(k_t)\right]\right\rvert^2 \left[1 - R_n(k_t)\, e^{2j\beta_n z}\right]\left[1 + R_n(k_t)\, e^{2j\beta_n z}\right]^*\right\}$
Absorption power, Eq. (7)	$S_a^n(z,\omega) = \frac{P_n}{\pi}\int_{-\infty}^{\infty} dk_t \left\{\frac{e^{-2\Im\{\beta_n\}z}}{\beta_n}\left\lvert\frac{e^{-j\beta_1 z'} - R_1(k_t)\, e^{j\beta_1 z'}}{1 - R_1(k_t)\,\widehat{R}_{-1}(k_t)}\left[\prod_{p=n}^{-2} \widehat{T}_p(k_t)\right]\right\rvert^2 \left[1 + \widehat{R}_n(k_t)\, e^{-2j\beta_n z}\right]\left[1 - \widehat{R}_n(k_t)\, e^{-2j\beta_n z}\right]^*\right\}$
Line source power, P_n	${}^{e}P_n = \frac{k_n Z_n \lvert {}^{e}I_0\rvert^2}{16}$; ${}^{m}P_n = \frac{k_n Y_n \lvert {}^{m}I_0\rvert^2}{16}$

3. RESULTS

The potential promise of our modeling approach, outlined in the previous section, is demonstrated through radiation pattern simulations, incorporating coherence effects, of a prototype device. A basic configuration of a five layer bottom-emitting (BE) OLED is selected [1]. The elementary device, specified in Table 3 and depicted in Fig. 2, corresponds to Fig. 1 (setting $M = 1$ and $N = 3$) with an electric line source excitation located at $z' = 20\,\text{nm}$, radiates typically at $\lambda \approx 600\,\text{nm}$ [17].

n	Layer Material	n_n	κ_n	d_n[nm]
-2	Silver	0.124	3.73	$-\infty$
-1	MEH-DOO-PPV	1.9	0.01	0
$+1$	MEH-DOO-PPV	1.9	0.01	200
$+2$	ITO	1.85	0.0065	300
$+3$	Glass	1.5	0	10^6
$+4$	Air	1	0	$+\infty$

Table 3: Geometrical and electrical properties of a prototype BE-OLED, corresponding to Fig. 1. Data is retrieved from [6, 17].

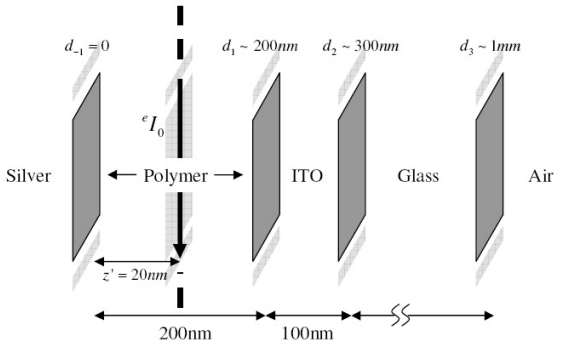

Figure 2: Physical configuration of the prototype BE-OLED specified in Table 3.

Radiation patterns of prototype BE-OLEDs with varying either glass layer thickness or coherence length are depicted in Fig. 3 and Fig. 4, respectively. While Fig. 3 patterns correspond to four glass layers with varying thickness, $\backsim 1\,\text{nm}$ to $\backsim 1\,\text{mm}$, and $L_c = 150\,\mu\text{m}$, Fig. 4 is associated with three coherence lengths, $5\,\mu\text{m}$ to $150\,\mu\text{m}$, whereas the glass layer thickness is set to $\backsim 1\,\mu\text{m}$.

It is readily observed that for device thickness (represented by the dominant glass thickness) much smaller than the coherence length, interference effects are noticeable whereas the reversed situation results in a quasi-Lambertian radiation pattern. Furthermore, these observations agree

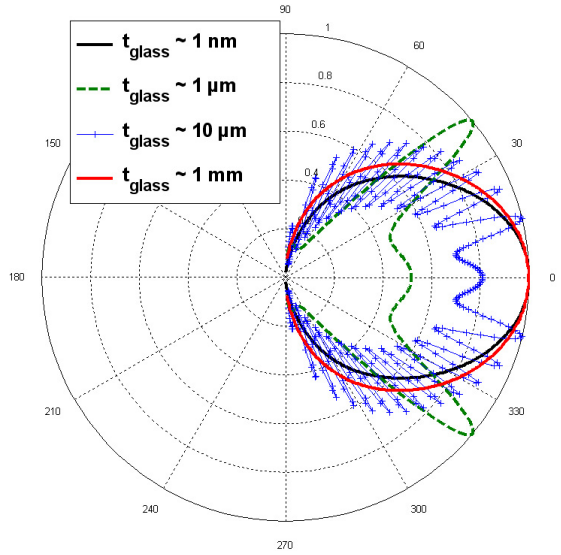

Figure 3: The effect of glass thickness on the OLED radiation pattern, for electric line source excitation, constant coherence length $L_c = 150\,\mu$m and four glass thickness values: $\backsim 1$ nm (black solid line), $\backsim 1\,\mu$m (green dashed line), $\backsim 10\,\mu$m (blue line with plus marker) and $\backsim 1$ mm (red solid line).

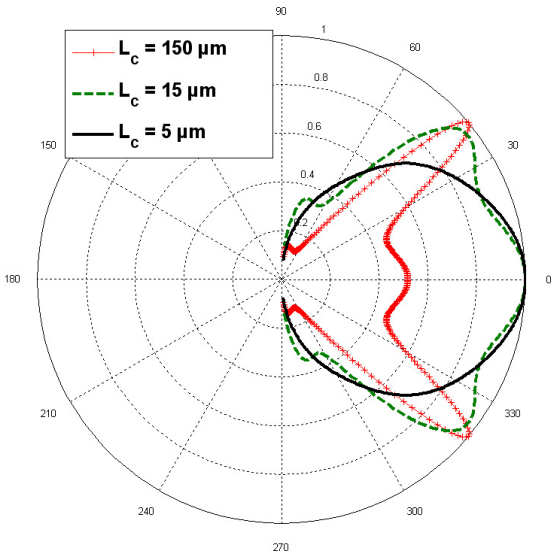

Figure 4: The effect of coherence length on OLED radiation pattern, for electric line source excitation, constant glass thickness of $\backsim 1\,\mu$m and three cohrence length values: 5 µm (black solid line), 15 µm (green dashed line) and 150 µm (red line with plus markers).

well with experimental measurements taken in the two limits, [9] and [6], respectively. Note that the two extremes correspond to radiation patterns which reflect either the device properties, i.e., thickness dependent interference, or the source characteristics, leading to spectral broadening dominated pattern.

4. CONCLUSION

A complete analysis for the electromagnetic radiation from two-dimensional OLEDs, incorporating temporal coherence effects, has been presented and verified through numerical simulations. The resultant analytical expressions preserve the physical intuition of the device optics and allow for an efficient implementation and design. Furthermore, as demonstrated for the prototype device, they establish a clear and simple relation between the device structure and the radiation pattern.

REFERENCES

1. Friend, R. H., R. W. Gymer, A. B. Holmes, J. H. Burroughes, R. N. Marks, C. Taliani, D. D. C. Bradley, D. A. Dos Santos, J. L. Brédas, M. Lögdlund, and W. R. Salaneck, "Electroluminescence in conjugated polymers," *Nature*, Vol. 397, 121–128, 1999.
2. Tessler, N., G. J. Denton, and R. H. Friend, "Lasing from conjugated-polymer microcavities," *Nature*, Vol. 382, No. 6593, 695–697, 1996.
3. Tessler, N., V. Medvedev, M. Kazes, S. H. Kan, and U. Banin, "Efficient near-infrared polymer nanocrystal light-emitting diodes," *Science*, Vol. 295, 1506–1508, 2002.
4. Forrest, S. R., "Active optoelectronics using thin-film organic semiconductors," *IEEE J. Sel. Top. Quantum Electron.*, Vol. 6, No. 6, 1072–1083, 2000.
5. Lu, M.-H. and J. C. Sturm, "Optimization of external coupling and light emission in organic light-emitting devices: Modeling and experiment," *J. Appl. Phys.*, Vol. 91, No. 2, 595–604, 2002.
6. Celebi, K., T. D. Heidel, and M. A. Baldo, "Simplified calculation of dipole energy transport in a multilayer stack using dyadic Green's functions," *Opt. Express*, Vol. 15, No. 4, 1762–1772, 2007.
7. Smith, L. H. and W. L. Barnes, "Using a low-index host layer to increase emission from organic light-emitting diode structures," *Org. Electron.*, Vol. 7, No. 6, 490–494, 2006.

8. Kim, J.-S., P. K. H. Ho, N. C. Greenham, and R. H. Friend, "Electroluminescence emission pattern of organic light-emitting diodes: Implications for device efficiency calculations," *J. Appl. Phys.*, Vol. 88, No. 2, 1073–1081, 2000.
9. Michelotti, F., G. Roma, A. Belardini, N. Danz, A. Pace, F. Sarto, and R. M. Montereali, "Micro-cavity organic light emitting diodes for biochip applications," *J. Non-Cryst. Solids*, Vol. 352, No. 23–25, 2476–2479, 2007.
10. Kahen, K. B., "Rigorous optical modeling of multilayer organic light-emitting diode devices," *Appl. Phys. Lett.*, Vol. 78, No. 12, 1649–1651, 2001.
11. Chance, R. R., A. Prock, and R. Silbey, "Molecular fluorescence and energy transfer near interfaces," *Adv. Chem. Phys.*, Vol. 37, 1–65, 1978.
12. Felsen, L. B. and N. Marcuvitz, *Radiation and Scattering of Waves*, 1st edn., Prentice-Hall, Englewood Cliffs, N.J., 1973.
13. Wolf, E., "Coherence and radiometry," *J. Opt. Soc. Am.*, Vol. 68, No. 1, 6–17, 1978.
14. Einziger, P. D., L. M. Livshitz, and J. Mizrahi, "Rigorous image-series expansions of quasistatic Green's functions for regions with planar stratification," *IEEE T. Antenn. Propag.*, Vol. 50, No. 12, 1813–1823, 2002.
15. Razansky, D., D. F. Soldea, and P. D. Einziger, "Bounds and estimates for power absorption in two-dimensional highly lossy configurations," *J. Appl. Phys.*, Vol. 95, No. 12, 8298–8308, 2004.
16. Saxena, K., D. S. Mehta, R. Srivastava, and M. N. Kamalasanan, "Spatial coherence properties of electroluminescence from Alq3-based organic light emitting diodes," *Appl. Phys. Lett.*, Vol. 89, No. 6, 061124, 2006.
17. Leger, J. M., S. A. Carter, B. Ruhstaller, H.-G. Nothofer, U. Scherf, H. Tillman, and H.-H. Hrhold, "Thickness-dependent changes in the optical properties of PPV- and PF-based polymer light emitting diodes," *Phys. Rev. B*, Vol. 68, No. 5, 054209, 2003.